Engineering Structures 114 (2016) 181–194

Contents lists available at ScienceDirect

Engineering Structures

journal homepage: www.elsevier.com/locate/engstruct

Flexural behaviour of composite steel–concrete beams utilising blind bolt shear connectors

Sameera Wijesiri Pathirana [a,*], Brian Uy [a], Olivia Mirza [b], Xinqun Zhu [b]

[a] Centre for Infrastructure Engineering and Safety, The University of New South Wales, Kensington, NSW 2052, Australia
[b] Institute for Infrastructure Engineering, University of Western Sydney, Penrith, NSW 2751, Australia

ARTICLE INFO

Article history:
Received 2 February 2015
Revised 14 January 2016
Accepted 19 January 2016
Available online 27 February 2016

Keywords:
Blind bolts
Composite beams
Demountable
Rigid plastic analysis
Finite element modelling
Push-tests
Shear-connectors

ABSTRACT

This paper investigates the feasibility of utilising blind bolts as shear connectors to develop demountable steel–concrete beams. The flexural behaviour of composite beams with two blind bolt types and welded stud connectors were experimentally investigated using full-scale beam specimens. A set of push-test specimens was tested based on the Eurocode 4 to compare the slip response of these connectors. The ultimate design loads of the test beams were calculated based on rigid plastic analysis (RPA) using the actual material properties. The beam experiments were simulated by using three-dimensional non-linear finite element models (FEMs). The material behaviour for concrete and steel in FEMs was described using concrete damage plasticity and steel plasticity models respectively. The FEMs were validated by comparing the load–midspan deflection curves of the beam specimens obtained from the experiments and modelling. The effects of the concrete compressive strength, steel yield strength and the shear connection ratio on the flexural behaviour of the composite beams were studied by utilising the validated FEMs. The experimental and numerical results suggest that the ability of the blind bolts to achieve and maintain composite action in steel–concrete beams under flexural loading is comparable to that of the welded stud connectors.

1. Introduction

Age is one of many factors that affect the condition and performance of infrastructure in terms of meeting current and future loading requirements. Recent records show that existing ageing infrastructure needs improvements to prolong their service life and to resist future loading [1]. New initiatives in the way that infrastructure is designed can address the problems of condition and performance to which age contributes. Introducing demountable composite beams is one such initiative. An increasing trend in investigating the feasibility of developing demountable composite steel–concrete beams can be identified in the open literature. These studies have primarily focused on investigating different types of bolted shear connectors that suit for this purpose. This paper identifies two types of blind bolting systems that have the potential to be utilised as shear connectors to develop demountable composite beams.

Welded stud connectors are widely used in composite steel–concrete beams. The availability of detailed research [2–5,6] and standard design methods have made these connectors very popular in the construction industry. Some of the problems associated with welded stud connectors have also been attempted to be addressed over the last few decades. Researchers such as Kim and Jeong [7] and Kim et al. [8] addressed the welding quality, structural safety, constructability and cost-effectiveness of new connector types over welded stud connectors. However, composite beams with these connectors cannot be effortlessly deconstructed without damaging the steel and concrete components. As a result headed shear studs cannot be utilised to develop deconstructable beams. This problem can be overcome by utilising bolted connectors in composite steel–concrete beams.

The two blind bolt types are referred to as BB1 and BB2 in this paper. Both are of M20 – grade 8.8 type bolts. The ability to be attached and detached from one side of a structure is one of the main aspects of these bolting systems that can be exploited to develop deconstructable composite beam systems. The advantages of these connectors are not limited to this aspect only. The bolt installation process that utilises power tools is much faster compared with the welded stud installation process. The installation process does not require heavy equipment to be run along the beams in which the bolts are fixed. Therefore the blind bolt installation process is less complex and faster when compared with that of welded stud connectors. Blind bolts can also be tightened to a

* Corresponding author. Tel.: +61 405 362 563.
E-mail address: i.wijesiripathirana@student.unsw.edu.au (S. Wijesiri Pathirana).

http://dx.doi.org/10.1016/j.engstruct.2016.01.057
0141-0296/

required torque with acceptable precision. Thus, the quality of the connection of blind bolts can be effectively assessed by nondestructive methods. Therefore the reliability of the quality assessment of the blind bolts is also much higher than that of welded stud connectors.

Due to the lack of detailed research and design guidelines bolted shear connectors are not widely used in composite beams. Nevertheless, using bolted connectors in composite beams continues to attract research interest due to their various benefits. Lam and Saveri [9] developed a demountable bolted shear connector using conventional welded headed stud connectors. They studied the load–slip behaviour of the demountable connector by carrying out a series of push-test experiments. The push-test specimens with bolted connectors were effortlessly deconstructed after the test. The test results reported that the demountable connectors demonstrated similar capacity and behaviour of the welded stud connectors. Pavlović et al. [10] carried out a series of push tests utilising welded studs and bolted connectors and compared the local behaviour of connectors in relation to the shear resistance, stiffness, ductility and failure modes. The authors carried out detailed finite element modelling and proposed a shear resistance reduction factor for bolted shear connectors. Both the above mentioned studies were limited to investigating the specific slip behaviour of bolted connectors in contrast to welded stud connectors. Kwon et al. [11] successfully utilised post installable bolted shear connectors to rehabilitate existing non-composite bridges. They used a type of friction grip bolt and double embedded nut shear connector in his investigation. Moynihan and Allwood [12] tested - three composite beams, of 2 m, 5 m and 10 m length, constructed utilising M20 bolts as demountable shear connectors. The first and second beams were practically tested for demountability. The beams were unloaded after subjecting to a certain service load before carrying out this test. The concrete slabs and the steel beams of these beams were fully separated and reassembled before loading to failure. They suggested that demountable composite beams can be safely used and practically reused. The bolted connector types utilised in the above mentioned research studies were different forms of standard nut-bolt assemblies. Installation of these connectors requires access from both the top and bottom sides of composite beams. Mirza et al. [13] compared the slip behaviour of blind bolts for the first time by carrying out a series of push-test experiments. They investigated the same blind bolt types considered in this paper. The experimental results suggested that these blind bolts demonstrated comparable behaviour and capacity to welded stud connectors. The dynamic behaviour of composite steel–concrete beams using removable blind bolts has also been investigated. Henderson et al. [14,15] tested the dynamic behaviour of steel–concrete composite beams with variable shear connection systems both experimentally and numerically. However, it can be clearly noted from this literature review that using blind bolts in composite beams has not been studied yet. Therefore this study takes the initiative to investigate the flexural behaviour of composite beams utilising blind bolts.

This paper investigates the ability of the blind bolts to achieve and maintain composite action in composite beams under static flexural loading. The ability of the connectors has been assessed and compared by investigating the flexural behaviour of composite beams in relation to the stiffness, strength and ductility. Three composite beams utilising the three connector types were tested for the ultimate load carrying capacity under static flexural loading. A non-composite beam specimen was also tested to use its results as a comparison to illustrate the ability of these connectors to achieve composite action in the composite beams. The slip behaviour of bolted connectors can be expected to be different to that of welded stud connectors. The slip behaviour of blind bolts is governed by several factors. They are yielding of the blind bolts, deformations of connector assemblies during loading and the existence of oversized bolt holes. This behaviour of bolted connectors has been reported by several research studies [10,13]. According to their results the initial stiffness of bolted shear connectors was lower compared with that of welded stud connectors. Three push-test specimens, one from each connector type, were tested along with the beam tests to study the slip behaviour of these connectors. The push-tests were carried out according to Eurocode 4 [16]. The load–deflection behaviour of the beam specimens and the load–slip characteristics of the push-test specimens were of primary concerns for the determination of the capacity and behaviour of shear connectors discussed in this paper.

Ultimate design loads of the beam specimens were estimated using the rigid plastic analysis (RPA) technique. Three-dimensional non-linear finite element models (FEMs) were developed using ABAQUS to simulate the full-scale beams. The FEMs were validated by comparing the load–deflection behaviour results of the experimental and numerical studies. A parametric study was carried out using the validated FEMs to study the flexural behaviour of the composite beams. The effects of shear connection ratio, the concrete compressive strength and the steel yield strength on the flexural behaviour of a composite beam were investigated. In addition, the slip of the concrete slab and steel beam of the composite beams along their interface was also studied using the FEMs. The FEMs were again validated using the experimental data of the longitudinal movement of the bottom steel flange of the beams for this analysis. The results obtained from full-scale beam and push-test experiments and also the analytical results from rigid plastic analysis (RPA) and finite element analysis (FEA) are presented and discussed in detail in this paper. The two blind bolt types used in this study are illustrated in Figs. 1a and 1b.

2. Experimental program

2.1. Full-scale beam tests

2.1.1. Details of the test specimens

Three composite beams and one non-composite beam specimens were constructed. The beam specimens were designed to represent a secondary beam used in high rise office building floors in accordance with the relevant Australian design standards. Fig. 2 illustrates the typical geometry of the test specimens. The main components of the beam that include the concrete slab and the steel beam were designed in accordance with AS 3600 [17] and AS 4100 [18] respectively. The composite design was carried out in accordance with AS 2327.1 [19] by following the load requirements given in AS 1170.1 [20]. Details of the beam specimens are provided in Table 1. Each composite beam contained twenty-seven shear connectors. This was the connector requirement for 50% shear connection ratio of the welded stud beam specimen based on the rigid plastic analysis (RPA). AS 2327.1 [19] specifies a lower limit of 50% shear connection ratio for the shear connection

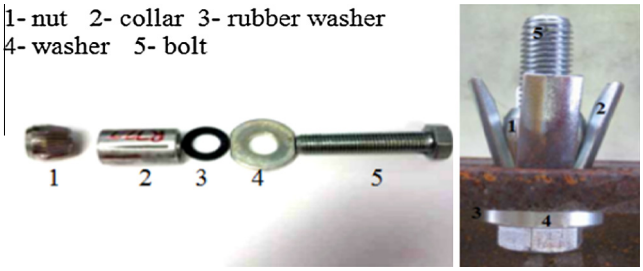

Fig. 1a. Blind bolt 1, BB1.

Fig. 1b. Blind bolt 2, BB2.

capacity for building floor designs. Shear connectors were placed in a staggered formation on the steel flanges with 230 mm centre to centre spacing between two consecutive connectors.

2.1.2. Instrumentation

The vertical deflections were measured throughout the test using Laser-potentiometers. The potentiometers were set up at mid span and under the loading points. These positions are denoted as L1, L2 and L3 in Fig. 3. Two linear variable displacement transducers (LVDTs) were installed at both ends of the beam to measure the horizontal displacement of the bottom steel flange. The force and stroke of the hydraulic jack and strains at selected points of the beam via attached strain gauges were also recorded.

2.1.3. Test setup and loading procedure

The test setup for the beam experiments is illustrated in Fig. 3. The test specimens were simply supported by a roller at one end and a pin at the other end. The load was applied by using a 1000 kN hydraulic jack. Four simply supported beams, given in Table 2, were tested under static loading conditions to failure. The beams were loaded at a constant rate of displacement of 2 mm per minute. This rate was increased at the end of the tests as the load–deflection curves began to plateau. Each beam was loaded at stages of 20%, 40%, 60% and 80% of their calculated ultimate design loads determined by the RPA. The beams were finally loaded up to their ultimate loads. The applied load of the beams plateaued and also the beams demonstrated considerable damages at this level of loading. After each loading stage, the beams were unloaded back to zero load and then loaded again to the next stage. The feasibility of using the BB1 connectors to develop demountable composite beams was investigated at the end of the second loading stage. Two bolts from both ends and one from the mid-span of the beam were unbolted and bolted back to the beam in this test. As the commercially available BB2 connectors have a round head instead of a hexagonal head this test was not carried out for the CBB2 beam at this stage.

2.2. Push-tests

The push-test specimens for this project were designed based on the standard push-test requirements given in Eurocode 4 [16]. The push-tests were conducted to investigate the load–slip behaviour of the three connector types. These push-test specimens utilised a 460 UB74.6 steel section and a 120 mm thick concrete slab reinforced with N12 bars. Each specimen contained four shear connectors, two on each flange, in a staggered formation representing the connector orientation of the corresponding full-scale beam specimens. The standard testing procedure for push-test specimens given in Eurocode 4 [16] was applied to test these specimens. According to this testing procedure, the load was first applied to the push-test specimens up to 40% of their expected failure loads. The load was then cycled 25 times between 5% and 40% of their expected failure loads. Finally the specimens were loaded until failure. The interface slip and uplift between the steel and concrete sections was measured at shear connector positions of the specimens using LVDTs. Throughout each test the force and stroke of the hydraulic jack was also measured.

3. Rigid plastic analysis (RPA)

The connector quantity for a fully composite beam specimen was calculated by carrying out RPA at the critical cross-sections. The critical-cross sections of the beam specimen were determined in accordance with the AS 2327.1 [19]. In this analysis all the structural elements that contribute to the flexural capacity at the critical, mid-span, cross-section of the beam were assumed to be fully yielded. An equivalent stress block was used in the compressive region of the concrete slab and the area of the concrete slab in tension was ignored. The ultimate flexural capacity of the partially composite test specimens were estimated according to a method proposed by Oehlers and Sved [21]. In this method the capacity of a partially composite beam was estimated using the linear interpolation method. The shear capacities of the connectors used in this analysis was evaluated in accordance with AS 2327.1 [19]. The shear connector type, shear capacities of the connectors and corresponding ultimate design moments and also the ultimate design loads of these beams are illustrated in Table 4.

4. Finite element analysis

Three dimensional non-linear finite element models (FEMs) were developed to simulate test beams. The load–deflection behaviour of the beam specimens was used to validate the FEMs. The flexural behaviour of composite beams was studied in detail by carrying out a parametric study using the validated FEMs. The concrete compressive strength, steel yield strength and shear connection ratio were the parameters considered in the parametric study.

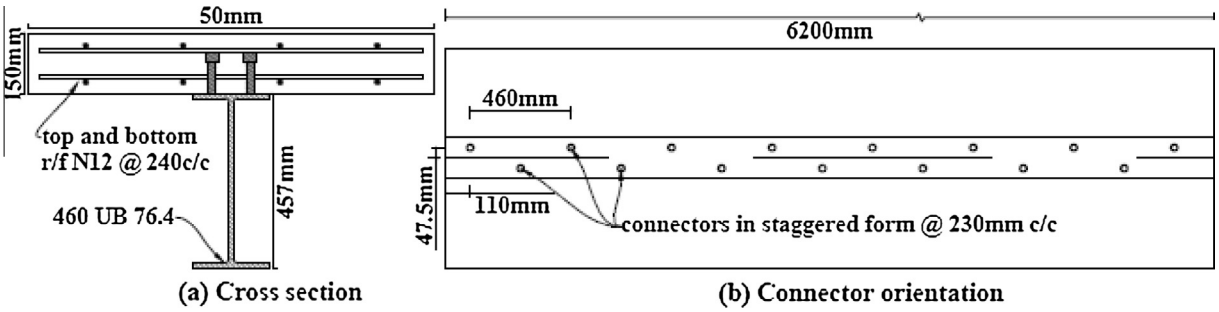

Fig. 2. Geometry of a typical beam specimen.

Table 1
Design details of the test specimens.

Span of the beam	6.0 m
Dead load (G)	4.33 kN/m
Impact load (Q)	4 kN/m
Width of the concrete slab	1 m
Thickness of the concrete slab	150 mm
Main bars top and bottom	N12 @ 240 mm c/c
Transverse bars	N12 @ 240 mm c/c top and bottom
Slab cover	50 mm
Steel section	460UB74.6
Connector distribution	230 mm c/c in staggered form
No of connectors in a beam specimen	27 no

Furthermore, the FEMs were used to investigate the load–slip response of these shear connectors inside the composite beams. The finite element models were developed and carried out using the commercial software, ABAQUS.

4.1. Material properties

Material property tests for steel and concrete were carried out to determine accurate mechanical properties of the actual materials used in the test specimens. Concrete cylinder tests were performed to evaluate compressive strengths and elastic moduli of concrete. These results are summarised in Table 2. Tensile tests were performed on coupons cut from the flange and web of the steel beams, shear connectors and reinforcing bars. These results are summarised in Table 3. The mechanical behaviour of these materials was defined using the uni-axial stress–strain relationship of these material types. The material properties of the components of the finite element models have been represented by constitutive laws and actual material property test data.

4.1.1. Concrete properties

A concrete damage plasticity model was utilised to describe the material behaviour for concrete. This model is intended primarily for the analysis of reinforced concrete structures and also designed for applications in which concrete is subjected to monotonic loading under low confinement pressure. The evolution of the yield (or failure) surface is controlled by tensile and compressive equivalent plastic strains linked to failure mechanisms under tensile and compressive loading [22]. The Concrete Damage Plasticity option is used in conjunction with Concrete Tension Stiffening and Concrete Compression Hardening options in ABAQUS. The flow potential and yield surface parameters have been defined using default values of ABAQUS in the concrete damage plasticity option. The material model introduced by Carreira and Chu [23] for normal weight concrete is used to define the elastic–plastic behaviour of concrete for the compressive region. The model is expressed by the following equations, and compression is assumed to be linear elastic up to $0.4f'_c$.

Table 2
Concrete material properties.

Age at testing (days)	Compressive strength (N/mm^2)	Elastic modulus (N/mm^2)
10	23	–
16	27	–
28	34	30,000
42	35	30,700
44	37	31,274

Table 3
Steel properties for different steel components.

Material type	Material property		
	E-modulus (N/mm^2)	Yield strength (N/mm^2)	Ultimate strength (N/mm^2)
Steel reinforcing	194,000	510	650
Steel beam	200,000	390	555
WS	183,000	390	515
BB1	207,000	860	920
BB2	187,000	795	900

$$\sigma_c = \frac{f'_c \gamma (\varepsilon_c/\varepsilon'_c)}{\left[\gamma - 1 + (\varepsilon_c/\varepsilon'_c)^{\gamma}\right]} \tag{1}$$

$$\gamma = \left[\frac{f'_c}{32.4}\right] + 1.55 \text{ and } \varepsilon'_c = 0.002 \tag{2}$$

where f'_c is the characteristic uniaxial compressive strength of concrete, σ_c is the uniaxial compressive stress and ε_c is the uniaxial strain of the concrete.

In this study, the stress–strain relationship of concrete in tension was assumed to be linear. The tensile stress of concrete increases linearly until concrete begins cracking in tension and decreases linearly to zero from that point. The ratio of the uniaxial tensile stress to the uniaxial compressive stress at failure is evaluated as 0.1 [24]. Fig. 4 illustrates the stress–strain relationship of concrete according to the compressive behaviour proposed by Carreira and Chu [23] and the uniaxial tensile stress–strain behaviour of concrete.

4.1.2. Steel properties

The stress–strain relationship of different steel materials was defined using material property test data in the finite element modelling. Steel materials exhibited elastic behaviour up to their yield points and this was followed by further yielding or strain hardening before fracture. The stress–strain relationships of these materials were converted into piecewise linear curves. Fig. 5 illustrates the stress–strain relationships of the steel materials used to model the steel beam, reinforcing steel, welded shear studs and the blind bolts BB1 and BB2 respectively.

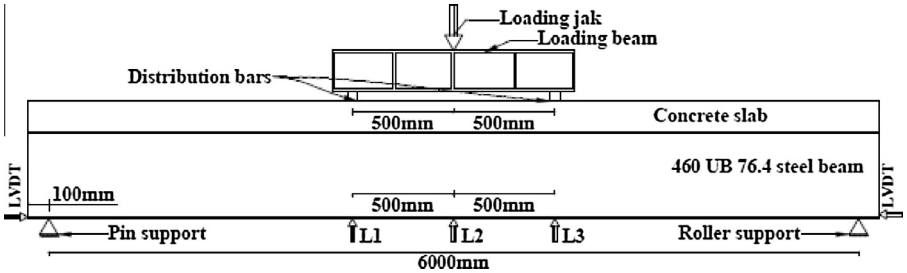

Fig. 3. Loading setup.

Table 4
Shear connection ratio, ultimate moment capacity and corresponding ultimate load capacity of different beam types according to the rigid plastic analysis.

Beam specimen	Shear connector type	RPA results		
		Shear capacity (kN)	U. design moment (kNm)	U. design load (kN)
CWS	Welded stud	100	747	597
CBB1	Blind bolt 1	110	809	647
CBB2	Blind bolt 2	110	809	647
NC	–	0	530	424

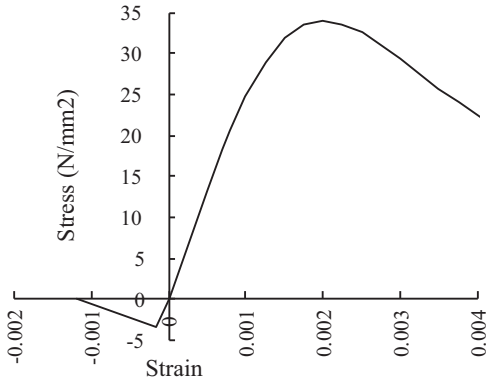

Fig. 4. Stress–strain relationship for concrete.

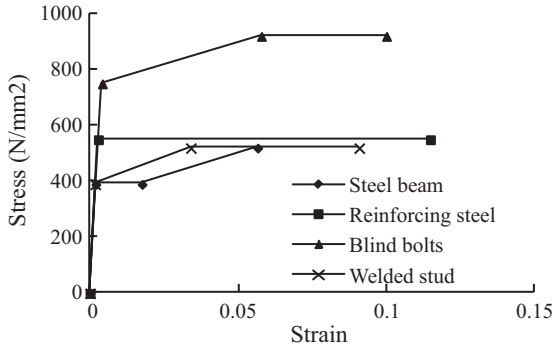

Fig. 5. Stress–strain relationship for different steel materials.

4.2. Geometry, element type and mesh

The test beams were symmetrical along their lengths. Therefore only a half of each beam along the length was modelled in the analysis to reduce the simulation time. The concrete slabs and steel beams were modelled using the eight-node linear hexahedral solid elements with reduced integration and hourglass control (C3D8R). Elements with reduced-integration were adopted as they could reduce computer run time. These elements were incorporated in a reasonably fine mesh in order to improve the accuracy of these models. The mesh sizes were also verified by carrying out a sensitivity analysis. The shear connectors were modelled using second order three-dimensional eight-node quadratic brick elements with reduced integration (C3D8R). The connectors were modelled to represent their actual geometric sizes and shapes within the limitations of the application. For this, the collar of the BB1 connector was modelled as a separate part which attached to the connector in the assembly module. However, the nuts of the bolted connectors were not considered as separate parts for this analysis. The reinforcing bars were modelled with two-node linear three-dimensional truss elements (T3D2). Fig. 6 illustrates the typical geometries and element types utilised to simulate the composite steel–concrete beam specimens and different connector types.

4.3. Contact properties, boundary conditions and load application

The interactions between different parts of the beam models were modelled using interaction and constraint options available in ABAQUS. The surface to surface interaction was used to model the contact between the steel beam, concrete slab and connector surfaces as is listed in Table 5. Furthermore, the details of the interaction between the bolted connectors and the other parts of the beam model are illustrated in Fig. 7a. Fig. 7b shows the region where Tie constraint is applied between the WS connectors and the steel beam top flange and also it shows the region where surface to surface interaction is applied between the welded headed connectors and the concrete slab. The normal and tangential behaviour between these contact surfaces was defined using the "Hard" and "Penalty" options respectively. The value used for the friction coefficient was 0.4. The embedded element technique was used to model the contact between reinforcing bars and concrete. In this technique perfect bond between embedded elements and host elements was chosen. This bonding will constrain the translational degree of freedom of the embedded nodes and will also avoid slip between the reinforcing bars and concrete. The nodes of the

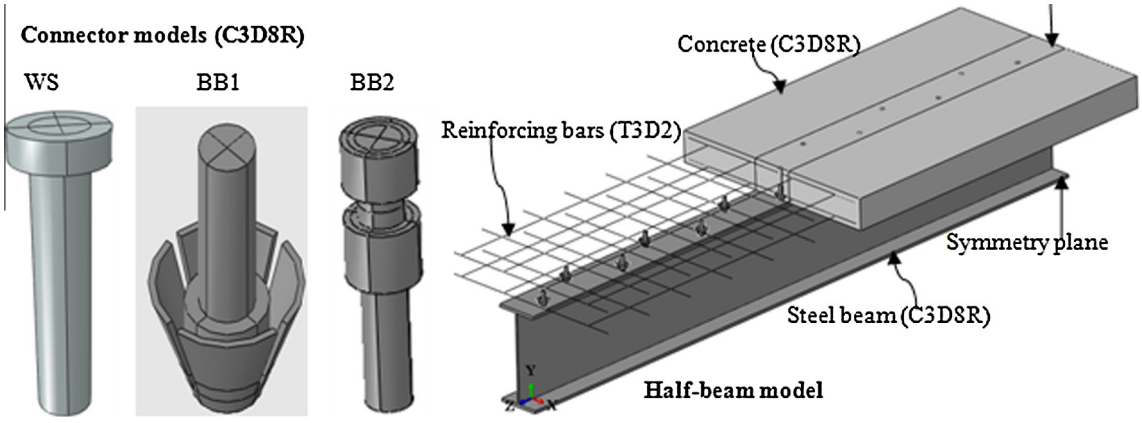

Fig. 6. Finite element model geometries and element types.

Table 5
Contact interaction between different parts of the beam models.

Part instance		Contact type		
1	2	CWS	CBB1	CBB2
Concrete slab	Steel beam	Interaction	Interaction	Interaction
Concrete slab	Reo	Embedded	Embedded	Embedded
Concrete slab	Connectors	Interaction	Interaction	Interaction
Concrete slab	Connector parts	–	Embedded	–
Steel beam	Connectors	Tie	Tie	Interaction

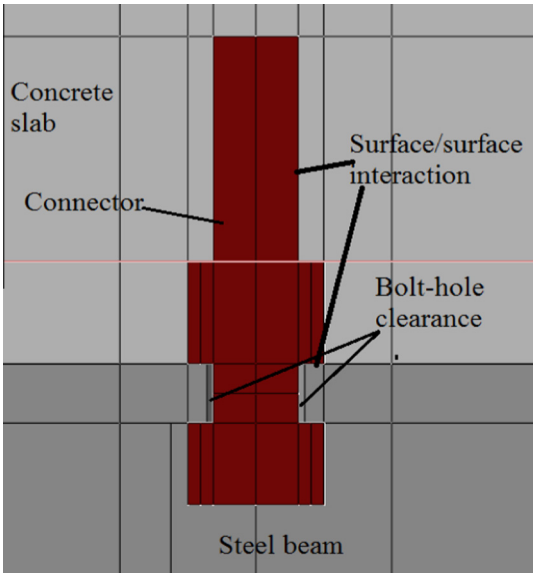

Fig. 7a. Details of the interaction between the bolted connectors and other components of the beam in FEM.

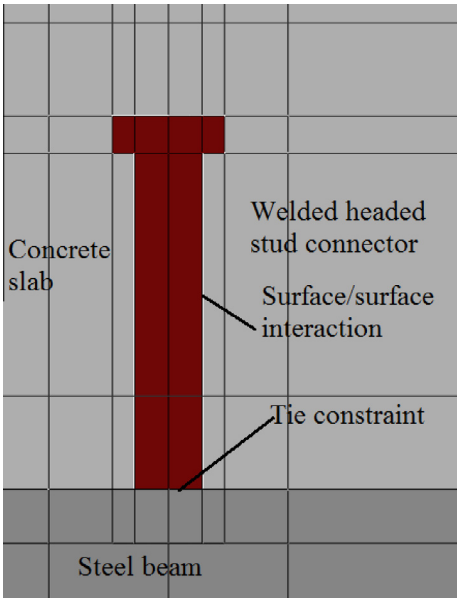

Fig. 7b. Details of the interaction between the WS connectors and other components of the beam in FEM.

concrete slab, reinforcing bars and steel beam on the plane of symmetry, at the mid-span of the beam were restricted from moving in the *z*-direction. The plane of symmetry is illustrated in Fig. 6. The load was applied to the model as an imposed vertical displacement

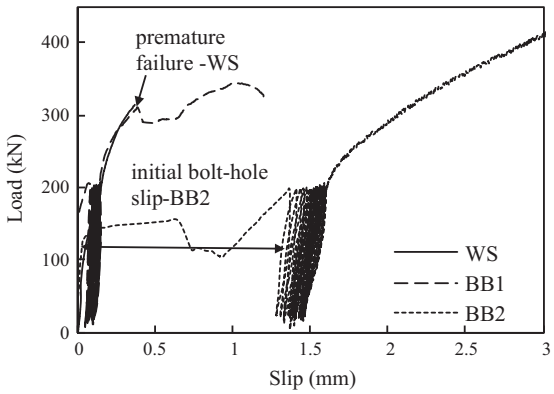

Fig. 8. Comparison of the load–slip curves of the push-test results.

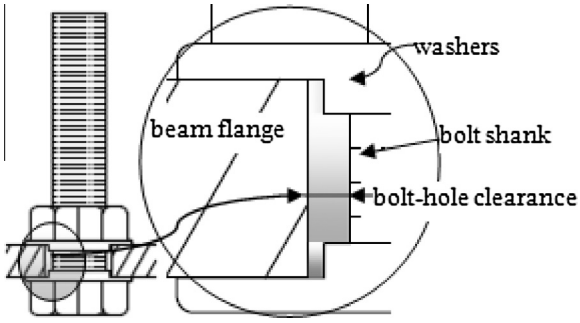

Fig. 9. Illustration of bolt-hole clearance.

on the concrete slab selecting a 50 mm wide loading strip across the width of the slab at a distance of 500 mm away from the centre-line of the beam to match the experimental setup. The deflection at the ultimate load of each test beam was considered as the maximum displacement of the corresponding model beam.

5. Results and discussion

5.1. Push-test results

Three push-tests, one specimen for each connector type, were carried out to compare the load–slip behaviour of these connectors in relation to the stiffness, strength and ductility. The failure modes were also observed. The load–slip relationship of each connector type is illustrated in Fig. 8. The BB1 connector demonstrated a much higher stiffness than the stiffness of the other two types of connectors. The BB2 connector exhibited a certain amount of slip at the beginning of the test. This initial slip can be attributed to the movement of the bolts within the oversized holes of the steel beam flange. The bolt-hole clearance that enables the initial slip of the BB2 connectors is illustrated in Fig. 9. The BB2 connector exhibited the highest ductility amongst the connectors and also the highest load carrying capacity before failure. The behaviour of the WS connectors was comparable with the BB2 connectors in terms of the initial stiffness but it demonstrated a sudden premature failure. This could be attributed to premature failure of poorly welded stud connectors. The bolted connectors exhibited concrete failure and the headed shear stud connectors exhibited weld failure.

5.2. Experimental results – full scale beam tests

The experimental load–deflection curves of the beam specimens have been modified by removing their intermediate loading–unloading curves. This measure was taken to enable a better

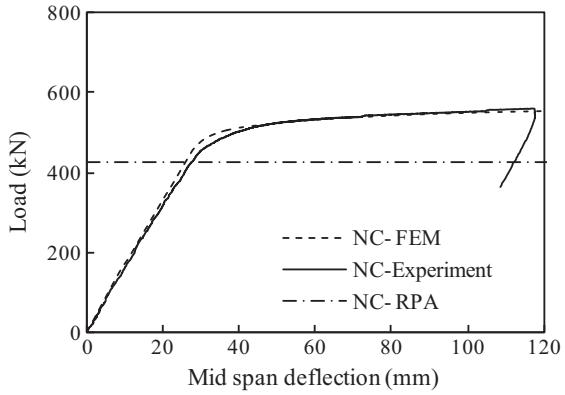

Fig. 10. Load–deflection curves for NC model and experiment.

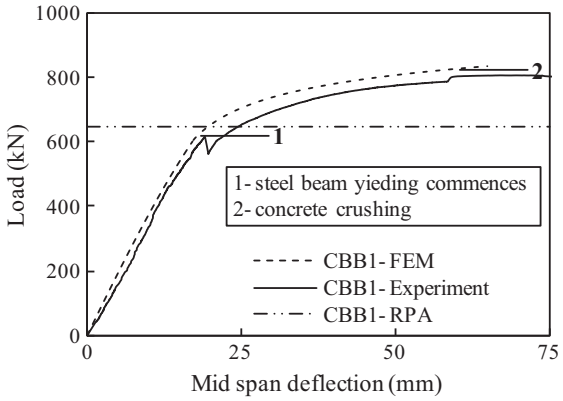

Fig. 13. Load–deflection curves for CBB1 model and experiment.

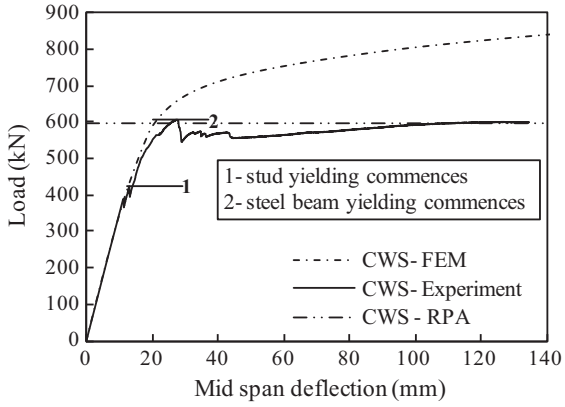

Fig. 11. Load–deflection curves for CWS model and experiment.

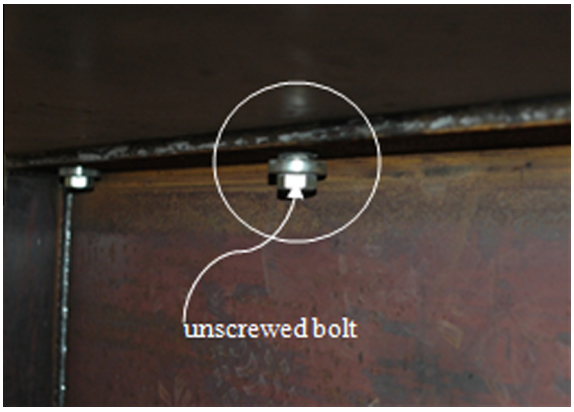

Fig. 14. Bolt after being loosened.

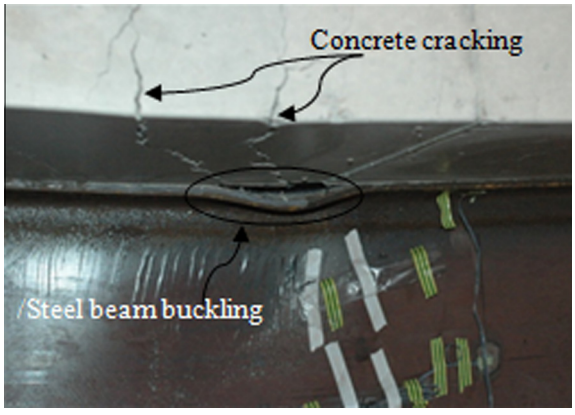

Fig. 12. Concrete cracking and steel beam buckling.

comparison between the load–deflection behaviour of these beams. In Figs. 10, 11, 13 and 15 these finite element model results are illustrated along with the corresponding experimental results.

5.2.1. Non-composite beam (NC)

Fig. 10 illustrates the load versus deflection relationship of the non-composite beam. Yielding of the beam began at a load of about 424 kN. Cracks on the concrete slab were first observed under the loading points at around 40% of the calculated ultimate design load. These cracks started to propagate to the top of the slab and spread toward the ends of the beam as illustrated in Fig. 17. The beam gradually achieved its maximum load carrying capacity of 558 kN, at 118 mm deflection.

5.2.2. Composite beam – welded studs (CWS)

The load–deflection curve presented in Fig. 11 illustrates the load versus mid span deflection relationship of the beam specimen during loading. A loud noise and a drop in the applied load were observed at a load of 380 kN and that was followed by a second load drop which occurred at a load of 420 kN. These noises and load drops can be attributed to premature failure of some of the welded stud connectors at the ends of the beam. This kind of stud failure in the early loading stages can be attributed to the poor quality of the welds of the welded stud connectors in the beam. The maximum load this beam could resist was 606 kN. This was slightly higher than the calculated ultimate design load of this beam which was 597 kN. Cracks on the concrete slab started to appear at around 80% of the calculated ultimate design load. The cracks first appeared at the mid span and under the loading points of the beam and gradually propagated to the top of the slab and toward both ends. The crack propagation in the concrete slab and local buckling of the top flange of the steel beam is illustrated in Fig. 12. This indicates that at this stage the shear connection system had lost its ability to maintain the required composite behaviour of the beam to resist further loading. The continuous deterioration of the shear connection system due to failure of connectors was one of the probable reasons for this type of premature failure of the beam specimen.

5.2.3. Composite beam – BB1 (CBB1)

The load versus deflection relationship of the composite steel–concrete beam containing the BB1 connectors is illustrated in Fig. 13. The feasibility of using the BB1 connectors to develop demountable composite beams was investigated at the end of

the second loading stage. Fig. 14 illustrates a bolt after being unbolted. No physical damage to the beam was observed and no considerable change in the load–deflection behaviour could be observed during the next stage of loading. These observations suggest that the ability of the shear connection system to achieve composite action in the beam had not been degraded by the unbolting and re-bolting process. At a load of about 615 kN a loud noise was noted and a significant drop in the load was observed which was likely to be due to fracture of a bolt. Cracks started to appear under the loading points at approximately 770 kN and this load was greater than the calculated ultimate design load. As the load–deflection curve began to plateau the loading rate was increased, which is visible in the graph after the beam reached 60 mm of deflection. The maximum load carrying capacity of the beam was 806 kN. Ripping off of the concrete around the bolts and also separation of the steel beam and the concrete slab along their interface was observed after this load. The failure mode of this beam is illustrated in Fig. 19.

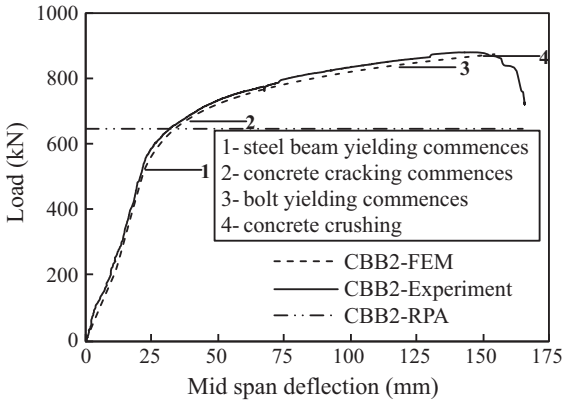

Fig. 15. Load–deflection curves for CBB2 model and experiment.

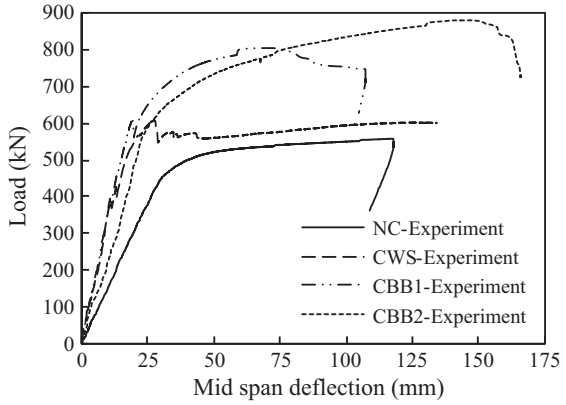

Fig. 16. Comparison of load–deflection curves.

5.2.4. Composite beam – BB2 (CBB2)

The load versus deflection relationship of the beam with the BB2 connectors is illustrated in Fig. 15. The beam demonstrated a much lower initial stiffness due to the movements of the bolts within the gap between the bolt shanks and the over-sized holes in the steel beam flange. A sharp increase in the stiffness can be observed at a load of about 200 kN. This can be attributed to the development of proper contact between the bolt shanks and the steel beam flange. The beam began to yield at a load of about 550 kN. Cracking of the underside of the concrete slab between the two loading points was observed at about 810 kN. The maximum load carrying capacity of the beam was 882 kN. The vertical deflection of the beam at this load was 150 mm. The beam failed due to concrete crushing at the top fibres between the two loading points as illustrated in Fig. 20.

5.2.5. Comparison of the load–deflection behaviour of the beams

Fig. 16 shows the comparison of the load–deflection curves of all the beams. All the composite beams exhibited a comparable initial stiffness. The CBB2 beam demonstrated a significant change in its stiffness at a load of about 100 kN due to the connectors slip within their oversized-holes. The stiffness of the CBB2 beam after this slip was comparable with that of the other two composite beams. The stiffness of the composite specimens was significantly higher than that of the non-composite beam specimen. The stiffness changes of the beams due to local effects of the connectors in relation to slipping and yielding are also visible in the load–deflection curves. All the three composite specimens exhibited yield loads higher than 500 kN. The CBB1 specimen recorded the highest yield load.

The ultimate load values of the beam specimens are summarised along with their theoretical and model results in Table 6. The beam specimens CBB2 and NC displayed the highest and the lowest ultimate loads respectively. Whilst the percentage (%) differences between theoretical and experimental ultimate load values are above 25% in other beam specimens, only the CWS specimen exhibited a 1% difference in that case. In the finite element model analysis, the CWS specimen recorded an ultimate load of 818 kN. This is almost a 37% increase compared with the calculated ultimate design load which is 597 kN. This value agrees with the values of the other beam models. These results suggest that premature failure had occurred in the CWS specimen during loading.

The beam specimens CBB2 and CBB1 demonstrated the highest and the lowest ductility respectively before failure. In contrast with the other two types of connectors the BB1 connector exhibited a very small slip during loading as is illustrated in Fig. 25. It seems that the expanded collar of this bolt type provided an additional inertia against the slip of these bolts inside the concrete slab. This action of the collar has further caused damages to the concrete slab by ripping off of the concrete material around the bolts as illustrated in Fig. 19. As a result, the CBB1 specimen exhibited a brittle type of failure.

Table 6
Comparison of ultimate strength results of different analysis methods.

Beam specimen	Ultimate flexural strength values obtained from different analysis methods (kN)			% of Difference of strengths	
	RPA result (F_{ut})	Experimental result (F_{ue})	FEM result (F_{um})	$\frac{\lvert F_{ue}-F_{ut}\rvert}{F_{ut}}$ (%)	$\frac{\lvert F_{um}-F_{ut}\rvert}{F_{ut}}$ (%)
CWS	597	606	818	1[a]	37
CBB1	647	806	806	25	25
CBB2	647	882	875	36	35
NC	424	558	557	31	31

[a] CWS shows the lowest percentage of difference between experimental and theoretical capacity.

5.3. Finite element model validation

5.3.1. Non-composite beam (NC)

The load versus mid-span deflection behaviour of the model and the test beam is illustrated in Fig. 10. The finite element model results showed good agreement with the test results in terms of their stiffness, strength and ductility. These results suggest that the finite element model is reasonably accurate and reliable in terms of predicting the behaviour of the test beam. Fig. 17 illustrates the tensile crack development under and near the loading points of the concrete beam of the model at around 40% of the calculated ultimate design load of the beam. The regions where the tensile stress in the concrete slab exceeds the ultimate tensile strength of the concrete are also illustrated in the figure. The crack development pattern of the concrete slab of this model is comparable with that of the test specimen.

5.3.2. Composite beam – welded studs (CWS)

Fig. 11 illustrates the load versus mid-span deflection behaviour of the finite element model and the test beam. The stiffness of the test beam and the model was in good agreement up to a load of 380 kN wherein the test beam exhibited a sudden drop in the load. The model recorded an ultimate load of 818 kN and this was a much higher value than that of the test beam. Fig. 18 illustrates the deformed beam and the welded stud connectors at 606 kN. The test beam exhibited a sudden failure at this loading level. The figure also illustrates the stress distribution of the connector at the end of the beam in the vertical direction (S22). This stress spectrum indicates that at this loading level the stud has been subjected to vertical stresses greater than their yield stress. These stresses are developed due to the vertical uplift of the studs during loading; acting on the surface of the shear studs in opposite directions creating an overturning moment on the studs. Further analysis revealed that the welded shear studs at the ends of the beam model started to yield at 400 kN. The steel beam yielding initiated at the bottom flange at a load of about 585 kN. A significant change in the stiffness of the specimen can be observed in both model and experimental curves after this point. The steel yielding points and concrete failure points of all the beam models are highlighted on their corresponding load–deflection curves.

5.3.3. Composite beam – BB1 (CBB1)

The FEM result in relation to the load–deflection behaviour illustrated in Fig. 13 suggests that the stiffness of both the model and the test specimens is in a very close agreement up to a load of 610 kN. Both specimens demonstrated yielding at about 610 kN and followed similar stiffness variations beyond this point. The stresses in the bolts never exceeded the yield limit before the beam reached its maximum load carrying capacity. Therefore the stiffness degradation was not significant prior to the steel beam yielding for this beam type. The test-specimen did not exhibit a considerable change in its stiffness during the initial loading steps. The initial slip of the bolts within their oversized-holes was negligible. Therefore the slip of these bolts within their holes was not taken into consideration in this analysis. Both the test and model beams demonstrated comparable strength and ductility. The failure mode exhibited by the test beam was also correctly predicted by the model. Fig. 19 illustrates these failures.

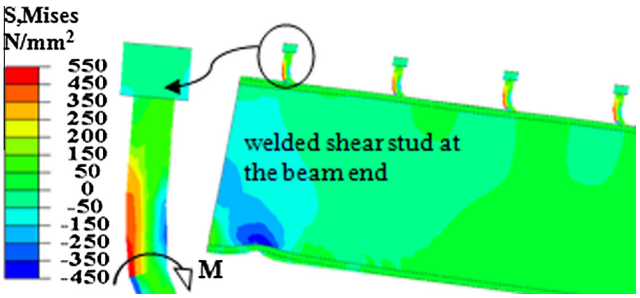

Fig. 18. The deformation of the beam and the welded headed studs at 606 kN.

5.3.4. Composite beam – BB2 (CBB2)

Fig. 15 illustrates the load versus mid-span deflection relationship of the finite element model and the test-specimen. Both specimens demonstrated comparable stiffness during loading. The FEM for this beam simulation was developed to demonstrate the initial slip of the BB2 bolts within their oversized-holes in the steel beam flange. It can be observed that both the specimens exhibited yielding at around 550 kN. The experimental and model results were in good agreement in terms of their strength and ductility as well. The ultimate loads recorded were 882 kN and 870 kN for the test and model specimens respectively. The change in the stiffness after yielding was quite similar for the two specimens. The connectors did not exhibit yielding before the ultimate load of the composite beam was reached. The model demonstrated concrete crushing failure in between the two loading points on the top side of the concrete slab. This failure mode of the model was very similar to the failure mode of the experimental beam as is illustrated in Fig. 20.

5.4. The interface-slip between the steel beam and the concrete slab

The horizontal movement of the bottom steel flange of each beam relative to their initial positions was measured during the experiment using LVDTs as illustrated in Fig. 3. These results are presented in Figs. 21–24 along with the corresponding model results. Except for the CWS specimen which exhibited premature failure, all the other three beam specimens demonstrated good agreement between the model and the experimental results. These results further suggested that the models were able to capture the actual behaviour of the test beams during loading. Therefore these

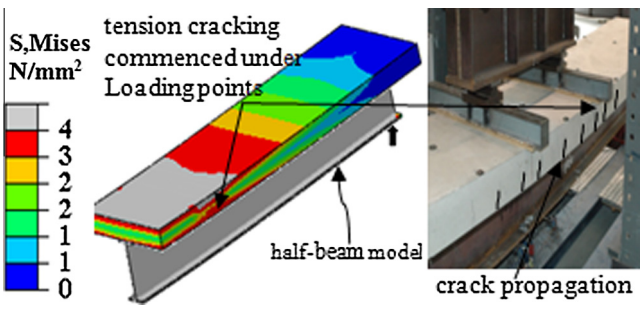

Fig. 17. Tension cracks developing in the concrete slab.

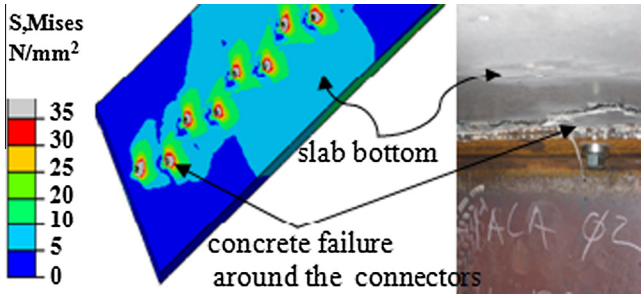

Fig. 19. Failure mode of CBB1.

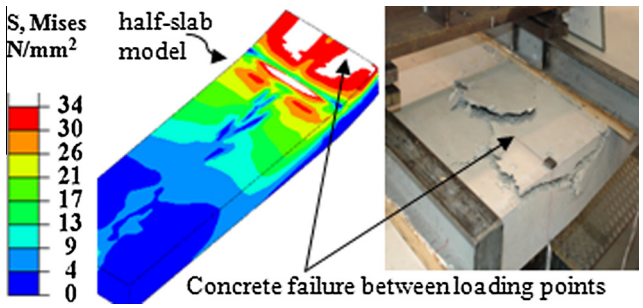

Fig. 20. Failure mode of CBB2.

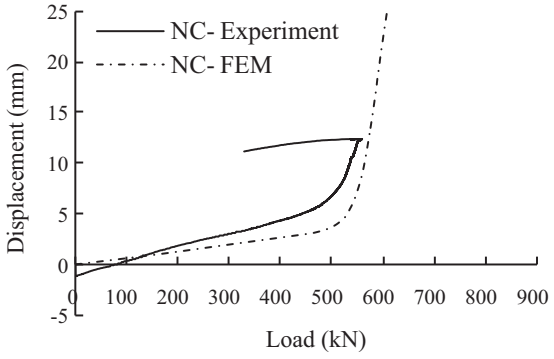

Fig. 21. Horizontal displacement of the bottom steel flange of the NC beam.

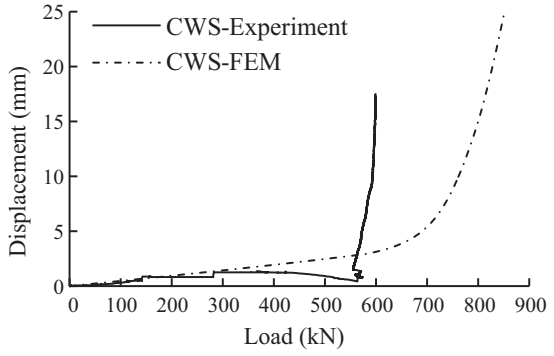

Fig. 22. Horizontal displacement of the bottom steel flange of the CWS beam.

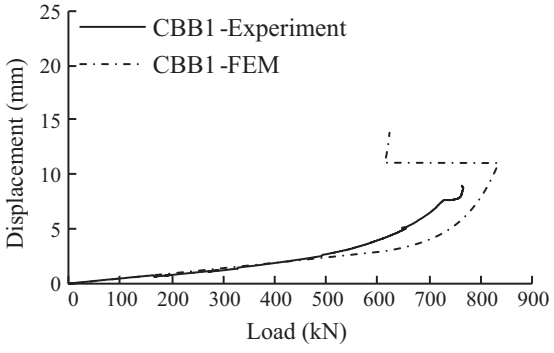

Fig. 23. Horizontal displacement of the bottom steel flange of the CBB1 beam.

models were used to study the effect of connector-slip response on the global behaviour of these beams.

Fig. 25 illustrates the slip between the steel beam top flange and the concrete slab along their interface of these beams during

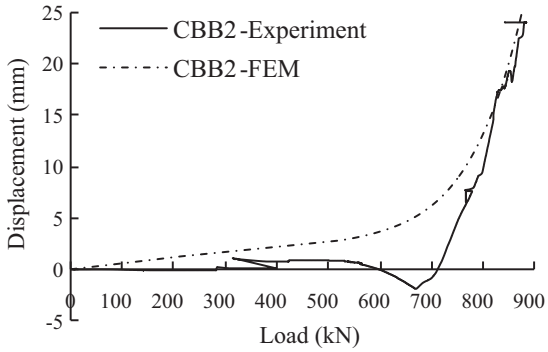

Fig. 24. Horizontal displacement of the bottom steel flange of the CBB2 beam.

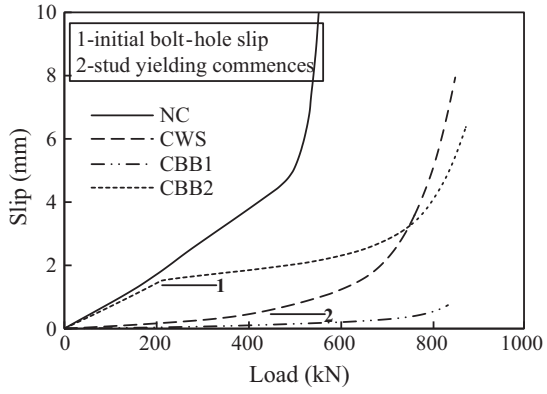

Fig. 25. Interface displacement of the concrete slab and steel beam during loading.

loading. The NC model demonstrated the highest sliding rate during loading. The sliding was almost linear until the top steel flange commenced yielding at about 500 kN. Beyond this limit the sliding rate increased significantly. The composite beam models exhibited significant reduction in the rate of sliding compared with that of the NC model. Significant changes in the sliding rate of the CWS model could be observed at about 400 kN and 550 kN. The connectors and the bottom steel flange of the CWS model commenced yielding at these points respectively. The slip between the concrete slab and the steel beam of the CBB1 beam was much lower compared with the other two composite beams. The BB1 connectors did not yield before the failure of the composite beam. The connectors did not also demonstrate considerable movement within the flange holes. The CBB2 specimen initially exhibited very low or zero composite behaviour until the connectors stopped moving within their oversized-holes at about 225 kN. Within this loading range the sliding rate of the CBB2 model was very close to that of the NC model. After this point the sliding rate reduced as the connectors began to develop composite action within the beam span. The BB2 connectors did not also yield during loading. The slip response of these connectors can be attributed to the presence of oversized bolt holes and local deformation of parts of the connectors such as collapsible washers. Only the welded stud connectors exhibited slip during loading due to yielding. The CWS model exhibited the highest slip among the composite beam specimens. These results suggest that the load–slip behaviour of shear connectors has a significant impact on the global behaviour of a composite beam.

5.5. Parametric studies

The effect of several parameters on the global behaviour of the composite beams was investigated using the FEMs. Concrete

Table 7
Effect of the steel yield strength on composite beams.

Beam type	Specimen (S_i)	Yield strength of the Steel beam (f_y) (N/mm^2)	Composite beam behaviour					
			Strength of the specimen		Stiffness	Ductility	(F_{ysi}/F_{ys250})	(F_{usi}/F_{us250})
			Yield load (F_{ysi}) (kN)	Ultimate load (F_{usi}) (kN)				
CBB2	S_{250}	250	380	642	No change	No change	1.0	1.0
	S_{300}	300	445	725			1.2	1.1
	S_{350}	350	535	875			1.4	1.4
	S_{400}	400	605	885			1.6	1.4
	S_{450}	450	675	963			1.8	1.5
CBB1	S_{250}	250	430	622	No change	No change	1.0	1.0
	S_{300}	300	505	715			1.2	1.1
	S_{350}	350	610	833			1.4	1.3
	S_{400}	400	680	896			1.6	1.4
	S_{450}	450	770	983			1.8	1.6
CWS	S_{250}	250	425	624	No change	No change	1.0	1.0
	S_{300}	300	502	706			1.2	1.1
	S_{350}	350	575	787			1.4	1.3
	S_{400}	400	650	861			1.5	1.4
	S_{450}	450	735	945			1.7	1.5

F_{ysi} = Yield strength of the composite beam corresponding to the specimen S_i.
F_{ys250} = Yield strength of the composite beam corresponding to the specimen S_{250}.

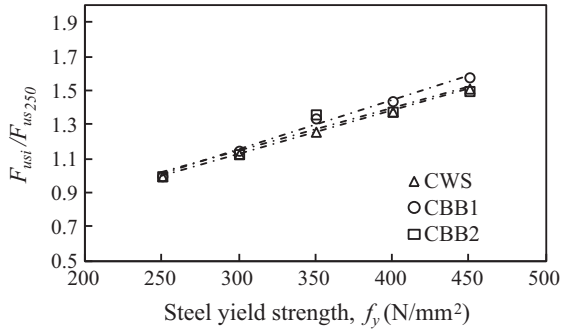

Fig. 26. Effect of steel yield strength (f_y) on the strength of composite beams.

compressive strength of the slab element, yield strength of the steel beam and number of connectors in the shear connection system of a particular beam are the key parameters that were considered in this study. The ability of these shear connector types to achieve composite action in steel–concrete beams was further investigated using these results.

5.5.1. Effect of steel beam strength

Table 7 illustrates the ultimate load capacities and yield loads of the beam models for different yield strengths of their steel beams. The standard yield strengths of steel 250 MPa, 300 MPa, 350 MPa, 400 MPa and 450 MPa values were considered in this study. Fig. 26 illustrates the effects of steel yield strength of the steel beam on the ultimate strength of these composite beams. According to these analysis results, the steel strength of a composite beam

Table 8
Effect of concrete strength on composite beams.

Beam type	Specimen (C_i)	Concrete strength (f'_c) (N/mm^2)	Composite beam behaviour					
			Strength of the specimen		Stiffness	Ductility	(F_{yci}/F_{yc20})	(F_{uci}/F_{uc20})
			Yield load (F_{yci}) (kN)	Ultimate load (F_{uci}) (kN)				
CBB2	C_{20}	20	502	825	Increase with the concrete strength	No change	1.00	1.00
	C_{25}	25	521	840			1.04	1.02
	C_{28}	28	535	860			1.07	1.04
	C_{32}	32	540	875			1.08	1.06
	C_{36}	36	547	880			1.09	1.07
	C_{40}	40	552	887			1.10	1.08
CBB1	C_{20}	20	602	816	Increase with the concrete strength	No change	1.00	1.00
	C_{25}	25	602	816			1.00	1.00
	C_{28}	28	602	816			1.00	1.00
	C_{32}	32	610	833			1.01	1.02
	C_{36}	36	615	840			1.02	1.03
	C_{40}	40	620	860			1.03	1.05
CWS	C_{20}	20	625	822	Increase with the concrete strength	No change	1.00	1.00
	C_{25}	25	635	835			1.02	1.02
	C_{28}	28	645	850			1.03	1.03
	C_{32}	32	660	860			1.06	1.05
	C_{36}	36	670	865			1.07	1.05
	C_{40}	40	675	884			1.08	1.08

F_{yci} = Yield strength of the composite beam corresponding to the specimen C_i.
F_{yc20} = Yield strength of the composite beam corresponding to the specimen C_{20}.

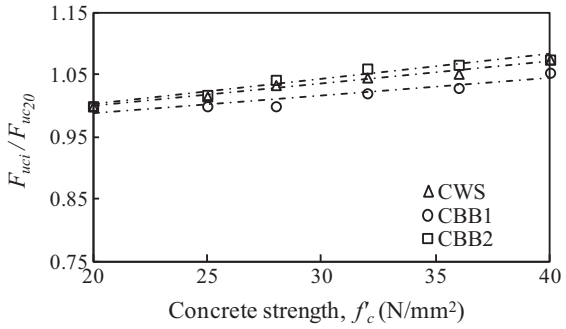

Fig. 27. Effect of concrete strength (f'_c) on the strength of composite beams.

has a very significant effect on the ultimate load carrying capacity of the beam. The overall stiffness of a composite beam is primarily governed by the material properties of its steel beam. The CBB1 specimen demonstrated a slightly higher increase in the ultimate load capacity for increasing steel yield strengths compared with the other two beams.

5.5.2. Effect of concrete slab strength

The standard concrete strength values considered in this analysis are detailed in Table 8. These values are the characteristic compressive strength values for normal weight concrete specified in most international design standards. The material properties in relation to their stress–strain behaviour for normal weight concrete were effectively modelled using the model proposed by Carreira and Chu [23] for normal weight concrete as discussed earlier in this paper. Fig. 27 illustrates the effects of concrete strength on the ultimate strength of these beams. These results suggest that the material strength of the slab of a composite beam affects the stiffness of the beam. A very small increase in the ultimate load values can also be observed for beams with higher concrete strengths. The maximum strength increment gained by any composite beam using C40 concrete was less than 10% of the strength of the same composite beam with C20 concrete. The effect of the concrete strength on the behaviour of these composite beams was comparable.

5.5.3. Effect of shear connection ratio

Shear connection ratios of 0, 0.25, 0.3, 0.4, 0.45, 0.5, 0.6, 0.7, 0.75, 0.85, 0.9 and 1 were considered for each beam type by changing the connector quantity of the beam. Tables 9–11 present the ultimate load capacities of the composite beam models for different shear connection ratios. The variation of the ultimate load carrying capacity with the shear connection ratio is illustrated in Fig. 28. These results demonstrated that the ultimate strength of a non-composite beam can be improved by more than 40% by increasing the shear connection ratio to approximately 0.25.

Table 9
Effect of shear connection ratio on CWS beam.

Beam type	Specimen (SC_i)	No of connectors	Shear connection ratio (β)	Composite beam behaviour					
				Strength of the specimen		Stiffness	Ductility	(F_{ysci}/F_{ysc0})	(F_{usci}/F_{usc0})
				Yield load (F_{ysci}) (kN)	Ultimate load (F_{usci}) (kN)				
CWS	SC_{52}	52	1.00	690	923	Increasing with the shear connection ratio	No change	1.47	1.69
	SC_{48}	48	0.90	686	918			1.46	1.68
	SC_{44}	44	0.80	680	913			1.45	1.67
	SC_{40}	40	0.75	655	898			1.39	1.64
	SC_{36}	36	0.65	647	884			1.38	1.62
	SC_{32}	32	0.60	640	878			1.36	1.61
	SC_{28}	28	0.50	615	861			1.31	1.57
	SC_{24}	24	0.45	602	852			1.28	1.56
	SC_{20}	20	0.35	590	827			1.26	1.51
	SC_{16}	16	0.30	570	815			1.21	1.49
	SC_{12}	12	0.20	562	792			1.20	1.45
	SC_0	0	0.00	470	547			1.00	1.00

F_{ysci} = Yield strength of the composite beam corresponding to the specimen SC_i.
F_{ysc0} = Yield strength of the composite beam corresponding to the specimen SC_0.

Table 10
Effect of shear connection ratio on CBB1.

Beam type	Specimen (SC_i)	No of connectors	Shear connection ratio (β)	Composite beam behaviour					
				Strength of the specimen		Stiffness	Ductility	(F_{ysci}/F_{ysc0})	(F_{usci}/F_{usc0})
				Yield load (F_{ysci}) (kN)	Ultimate load (F_{usci}) (kN)				
CBB1	SC_{52}	52	1.00	624	865	Increasing with the shear connection ratio	No change	1.33	1.58
	SC_{48}	48	0.90	620	864			1.32	1.58
	SC_{44}	44	0.80	620	864			1.32	1.58
	SC_{40}	40	0.75	618	858			1.31	1.57
	SC_{36}	36	0.65	615	849			1.31	1.55
	SC_{32}	32	0.60	612	847			1.30	1.55
	SC_{28}	28	0.50	610	835			1.30	1.53
	SC_{24}	24	0.45	605	830			1.29	1.52
	SC_{20}	20	0.35	592	819			1.26	1.50
	SC_{16}	16	0.30	585	792			1.24	1.45
	SC_{12}	12	0.20	570	764			1.21	1.40
	SC_0	0	0.00	470	547			1.00	1.00

F_{ysci} = Yield strength of the composite beam corresponding to the specimen SC_i.
F_{ysc0} = Yield strength of the composite beam corresponding to the specimen SC_0.

Table 11
Effect of shear connection ratio on CBB2.

Beam type	Specimen (SC_i)	No of connectors	Shear connection ratio (β)	Composite beam behaviour					
				Strength of the specimen		Stiffness	Ductility	(F_{ysci}/F_{ysc0})	(F_{usci}/F_{usc0})
				Yield load (F_{ysci}) (kN)	Ultimate load (F_{usci}) (kN)				
CBB2	SC_{52}	52	1.00	568	918	Increasing with the shear connection ratio	No change	1.21	1.68
	SC_{48}	48	0.90	565	917			1.20	1.68
	SC_{44}	44	0.80	562	914			1.20	1.67
	SC_{40}	40	0.75	560	910			1.19	1.66
	SC_{36}	36	0.65	555	925			1.18	1.69
	SC_{32}	32	0.60	550	897			1.17	1.64
	SC_{28}	28	0.50	540	884			1.15	1.62
	SC_{24}	24	0.45	530	866			1.13	1.58
	SC_{20}	20	0.35	520	857			1.11	1.57
	SC_{16}	16	0.30	510	828			1.09	1.51
	SC_{12}	12	0.20	500	794			1.06	1.45
	SC_0	0	0.10	470	547			1.00	1.00

F_{ysci} = Yield strength of the composite beam corresponding to the specimen SC_i.
F_{ysc0} = Yield strength of the composite beam corresponding to the specimen SC_0.

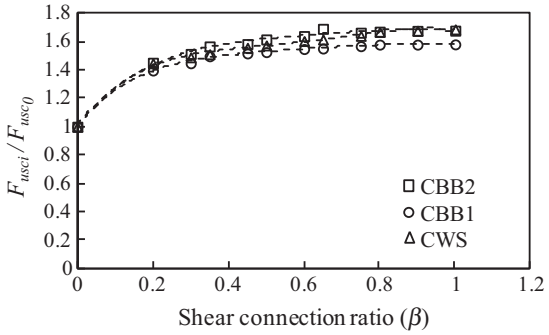

Fig. 28. Strength variation of composite beams with the shear connection ratio, β.

6. Conclusions

Four full-scale beam specimens were tested under static loading conditions to study the flexural behaviour of composite steel–concrete beams utilising three different connector types and one non-composite steel concrete beam. Four 3-dimensional non-linear finite element models (FEMs) were developed to simulate the beam specimens. FEMs were validated using the load–deflection relationship results of the test beams. A parametric study was carried out using the validated FEMs.

- Composite steel–concrete beams with the blind bolt connectors exhibited comparable behaviour to composite beams with welded stud connectors in relation to the stiffness, strength and ductility. The composite beam with the BB2 connectors demonstrated the highest strength and ductility, whilst the composite beam with the BB1 connectors exhibited the highest stiffness.
- All the beam types recorded much higher ultimate loads than their ultimate design loads calculated using the rigid plastic analysis (RPA). The welded headed stud beam failed prematurely possibly due to the poor weld quality of welded stud connectors and recorded the lowest increment in the ultimate load over its calculated ultimate design load. This paper has revealed that the blind bolts can be more reliable in achieving and maintaining composite action in new composite steel–concrete beams compared with welded stud connectors.
- Several blind bolts selected from critical sections of the CBB1 beam were able to be unbolted and retightened successfully. The beam was first loaded up to 40% of the calculated ultimate design load and then unloaded before carrying out this test. No degradation of the shear connection was observed during further loading of the beam. The bolts had also not been deformed due to yielding during loading according to the FEM results. These results suggest that this blind bolt type can be utilised to develop deconstructable composite beam systems.
- The global behaviour of these beams for different steel strengths, concrete strengths and shear connection ratios were investigated by carrying out parametric studies using the FEMs. The results showed that all the beam types demonstrate a very similar behaviour in responding to the changes of these parameters. The capacity and behaviour of the bolted connectors of the composite beams subject to these effects are comparable to that of the welded stud connectors.
- The parametric analysis results reported that a greater than 40% of strength increment over its original strength can be achieved for a composite steel–concrete beam by improving its shear connection ratio from 0 to 0.25, irrespective of the connector type.
- The welded stud connectors and the BB2 connectors demonstrated considerable slip in the composite beams during loading and the BB1 connectors exhibited the lowest slip. The blind bolt connectors did not yield during loading. The slip response of the bolted connectors can be attributed to the presence of oversized bolt holes and deformation of connector parts. Only the welded stud connectors exhibited slip during loading due to yielding. The CBB2 and CWS beams demonstrated a higher ductility compared with the CBB1 beam specimen. The results showed that the stiffness and ductility of a composite beam is greatly influenced by the load–slip behaviour of its shear connectors.
- The experimental and finite element model results suggest that these innovative blind bolting systems demonstrate comparable behaviour and capacity in achieving and maintaining composite action in new composite steel–concrete beams to that of the welded stud connectors. These results also suggest that these blind bolting systems would be a very good alternative as innovative shear connectors that can be employed to develop demountable steel–concrete composite beam systems.

Acknowledgements

The authors would like to acknowledge the financial support provided by the Australian Research Council's Discovery Projects funding scheme DP110101328. The experimental work was carried

out at the University of Western Sydney and the technical staff led by Dr. Mithra Fernando is gratefully acknowledged. The first author was supported by an Australian Postgraduate Research Award at the University of New South Wales and this is also gratefully acknowledged.

References

[1] Engineers Australia. Australian Infrastructure Report Card; 2010. <http://www.engineersaustralia.org.au/infrastructurereport-card>.
[2] Ollgaard JG, Slutter RG, Fisher JW. Shear strength of stud connectors in lightweight and normal-weight concrete. J ACI Struct 1971;8:55–64.
[3] Oehlers DJ, Coughlan CG. The shear stiffness of stud shear connections in composite beams. J Constr Steel Res 1986;6:273–84.
[4] Shim CS, Lee PG, Yoon TY. Static behaviour of large stud shear connectors. Eng Struct 2004;26:1853–60.
[5] Mirza O, Uy B. Behavior of headed stud shear connectors for composite steel–concrete beams at elevated temperatures. J Constr Steel Res 2009;65:662–74.
[6] Mirza O, Uy B. Effects of strain regimes on the behaviour of headed stud shear connectors for composite steel–concrete beams. Adv Steel Constr 2010;6(1):635–61.
[7] Kim HY, Jeong YJ. Experimental investigation on behavior of steel–concrete composite bridge decks with perfobond ribs. J Constr Steel Res 2006;62(5):463–71.
[8] Kim YH, Lee HCS, Yoon SJ. Experimental and analytical investigation on the hat shaped shear connectors in the steel–concrete composite flexural member. Int J Steel Struct 2011;11(1):99–107.
[9] Lam D, Saveri E. Shear capacity of demountable shear connectors. In: Proceedings of the 10th international conference on advances in steel concrete composite and hybrid structures; 2012.
[10] Pavlović M, Marković Z, Veljković M, Buđevac D. Bolted shear connectors vs. headed studs behaviour in push-out tests. J Constr Steel Res 2013;88:134–49.
[11] Kwon G, Engelhardt MD, Klingner RE. Behavior of post-installed shear connectors under static and fatigue loading. J Constr Steel Res 2009;66(4):532–41.
[12] Moynihan MC, Allwood JM. Viability and performance of demountable composite connectors. J Constr Steel Res 2014;99:47–56.
[13] Mirza O, Uy B, Patel N. Behavior and strength of shear connectors utilising blind bolting. Paper presented to the 4th international conference on steel and composite structures: Sydney; 2010, 21–23 July.
[14] Henderson IEJ, Zhu XQ, Uy B, Mirza O. Dynamic behaviour of steel–concrete composite beams with variable shear connection systems. Part I: experimental study. J Eng Struct 2015;103:298–307.
[15] Henderson IEJ, Zhu XQ, Uy B, Mirza O. Dynamic behaviour of steel–concrete composite beams with variable shear connection systems. Part II: modelling and comparison. J Eng Struct 2015;103:308–17.
[16] Eurocode 4: design of composite steel and concrete structures, part 1.1 general rules and rules for buildings, DDENV 1994-1. European Committee for Standardisation (CEN); 1992.
[17] Standards Australia, AS 3600-2009. Concrete structures. Code of practice for design. Standards Australia International Ltd; 2009.
[18] Standards Australia, AS 4100-1998. Steel structures. Code of practice for design. Standards Australia International Ltd; 1998.
[19] Standards Australia, AS 2327.1-2003. Composite structures part 1: simply supported beams. Standards Australia International Ltd; 2003.
[20] Standards Australia, AS 1170.1-2002. Structural design actions part 1: permanent, imposed and other actions. Standards Australia International Ltd; 2002.
[21] Oehlers DJ, Sved G. Composite beams with limited-slip-capacity shear connectors. J Struct Eng 1995;121:932–8.
[22] ABAQUS documentation, version 6.10. USA: Hibbitt, Karlsson and Sorensen; 2010.
[23] Carreira D, Chu K. Stress–strain relationship for plain concrete in compression. J ACI Struct 1985;82(11):797–804.
[24] Liang QQ, Uy B, Bradford MA, Ronagh HR. Ultimate strength of continuous composite beams in combined bending and shear. J Constr Steel Res 2004;60(8):1109–28.